Influence of radio frequency waves on the interchange stability in HANBIT mirror plasmas

Hogun Jhang, S. S. Kim, S. G. Lee, B. H. Park and J. G. Bak

Korea Basic Science Institute, 52 Yeoeun-dong, Yusung-Gu, Daejeon 305-333, Korea

e-mail: hgjhang@kbsi.re.kr

Abstract. Experimental and theoretical studies are made of the influence of high frequency radio frequency (rf) waves upon interchange stability in HANBIT mirror plasmas. An emphasis is put on the interchange stability near the resonance region, $\omega_0 \approx \Omega_i$, where ω_0 is the angular frequency of the applied rf wave and Ω_i is the ion cyclotron frequency. Recent HANBIT experiments have shown the existence of the interchange-stable operation window in favor of $\omega_0/\Omega_i \leq 1$ with its sensitivity on the applied rf power. A strong nonlinear interaction between the rf wave and the interchange mode has been observed with the generation of sideband waves. A theoretical analysis including both the ponderomotive force and the nonlinear sideband wave coupling has been developed and applied to the interpretation of the experiments, resulting in a good agreement. From the study, it is concluded that the nonlinear wave-wave coupling process is responsible for the rf stabilization of the interchange modes in HANBIT mirror plasmas operating near the resonance condition.

1. Introduction

Studies of interactions between externally applied radio frequency (rf) waves and collective modes of a confined plasma is a subject of not only theoretical but also practical importance in plasma physics since most of magnetic confinement devices employ high power rf waves for the purposes of plasma production and heating. Especially, the stabilization of interchange modes in magnetic mirror plasmas by the application of rf waves has attracted researchers owing to its potential advantages on mirror plasma operation.

It has been reported that rf waves had influence upon the interchange stability in mirror plasmas by the generation of a radial equilibrium ponderomotive force (EPF)[1-7] and the nonlinear sideband wave coupling (SBC) process[8-9]. The radial amplitude gradient of the rf wave generates the EPF, which is negative or positive depending on the sign of the gradient and the ratio $\gamma=\omega_0/\Omega_i$, where, ω_0 is the angular frequency of the rf wave and Ω_i, is the ion cyclotron frequency. If the direction of the EPF coincides with that of the effective gravitational force driving interchange modes, it has the destabilizing influence on the interchange modes while the opposite results in the stabilizing effects on them. The physical mechanism of the SBC process is analogous to the nonlinear parametric process. The nonlinear coupling between the interchange mode and the pump rf wave generates sideband waves with wave vectors $\mathbf{k}_\pm = \mathbf{k}_0 \pm \mathbf{k}$ and frequencies $\omega_\pm = \omega_0 \pm \omega$. Here, $\mathbf{k}$ and ω denote the wave vector and the frequency of the interchange mode involved, respectively, and $\mathbf{k}_0$ is the wave vector of the rf wave. Then, the nonlinear beating of the rf wave with the sideband waves produces a low frequency ponderomotive force, affecting the interchange stability of the plasma[9]. Physically, the ponderomotive force generated by this nonlinear process is interpreted as the perturbed force due to the distortion of the pump wave structure by the collective motion of the plasma[11]. Since both effects will be concomitant in a single plasma discharge, it is of importance to keep both effects for the interpretation of experimental results[10-12].

Most of previous experimental[1-5] and theoretical[6,7] analyses have attributed the observed

improvement of the interchange stability to the rf-generated EPF. The efficacy of the SBC process on interchange stability has been regarded to be weak or negligible[12]. In the present study, we report experimental and theoretical observations in the HANBIT mirror device that the nonlinear rf-interchange mode interaction is the dominant process for determining the stability near the ion cyclotron resonance region implying $|\gamma-1|\leq 0.1$, in contrast to the previous conclusions.

2. The HANBIT device and experimental setup

The HANBIT device is a magnetic mirror machine, consisting of a central cell of simple mirror geometry, an anchor cell, a plug cell, a fan-out tank and a cusp tank[13]. The central cell length is 420 *cm*. The rf antenna used in the present experiments is connected to a 500 *kW* rf transmitter the frequency of which is fixed at 3.5 *MHz* in normal operations. The antenna is located at (*r, z*)=(20.0, -45.0) in the central cell, where *r* and *z* represents the radial and axial position in *cm* unit, respectively. It is a copper cylinder the current path and the resulting rf-plasma coupling of which are similar to those of Nagoya Type-III antenna[14]. In typical HANBIT discharges, the rf power is applied from time t=0 to its desired value during 20 *msec* ramp up phase for plasma production, sustained for 180 *msec*, and ramped down for 30 *msec*. The midplane magnetic field is in the range of $0.22 < B_0$ (T) < 0.24 with the mirror ratio of ~10. The baseline pressure is $\sim 1.0\times10^{-4}$ *mtorr*. The neutral pressure in the central cell is $\sim 1.0\times10^{-2}$ *mtorr*, making the effects of ion-neutral collisions on interchange modes non-negligible ($\nu_i \sim 10$ *kHz*). Two gas boxes that are located at $z=\pm 100$ *cm* provide the hydrogen fuel puffing for the plasma initiation.

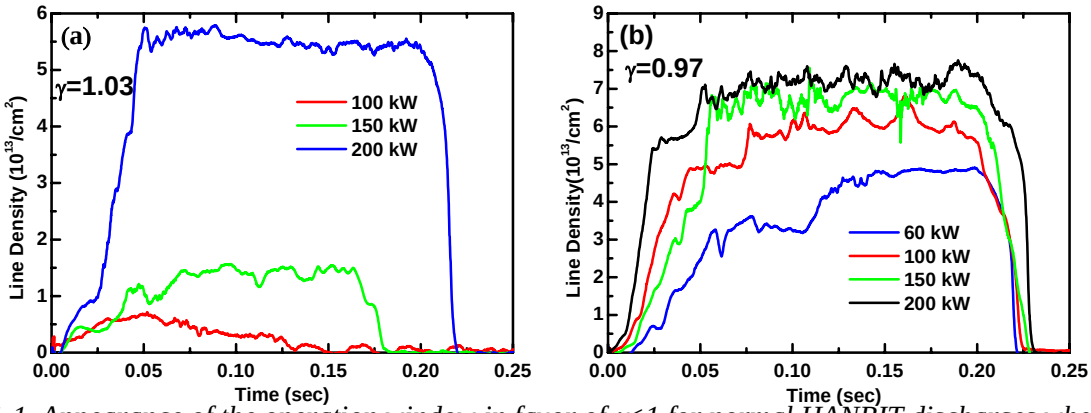

FIG. 1. Appearance of the operation window in favor of $\gamma<1$ for normal HANBIT discharges when (a) $\gamma=1.03$ and (b) $\gamma=0.97$.

In normal HANBIT discharges, we have observed the operation window within which a plasma discharge is carried out successfully, in a reproducible manner. A successful plasma discharge is obtained with the good line density behavior when the discharge condition is within the operation window, whereas the discharge is brought to an end by either the plasma production failure or the plasma termination during the operation when the condition is outside of it. The operation window has been found to be a sensitive function of the applied rf power and the value $\gamma=\omega_0/\Omega_i$ with a preference for $\gamma\leq 1$. Increase of rf power generally results in the slight expansion of the operation window into $\gamma \geq 1$ region while the decrease of it gives rise to the reduction of the operation window. Figure 1 shows the appearance of the operation window in normal discharges described above. The existence of the operation window was attributed to the rf effects on interchange stability although the exact mechanism leading to

the stabilization had not fully investigated. In the experiments reported here, we operated the device in the simple mirror geometry by turning off the anchor coil current to eliminate undesirable influences from the anchor fields on the rf wave propagation and interchange stability. Then, it is expected that the interchange stability depends only on rf characteristics and the confining magnetic fields.

Probe systems in the HANBIT device[15] are used as main diagnostic tools in this study. There are five arrays of fixed edge probes along the axial direction of the central cell, two of which are used to measure the azimuthal and parallel characteristics of the density fluctuation with 800 *kHz* sampling rate. The first array (array I) is located at (r, z)=(8.0, 204.8) (near the mirror throat) and the other one (array IV) is placed at (r, z)=(16.0, -99.9). Each array has eight single probe tips at a fixed radial position. A triple Langmuir probe system, which is movable in the radial direction, is placed at the midplane of the central cell. The system has triple probe tips, the dimension of which is the same as that of the fixed edge probe. It was used for the measurement of radial electron temperature and density profiles of the central cell plasma. The profile measurement was carried out on a shot by shot basis. Thus, a careful after-shot analysis has been performed to ensure the identity of each experiment. A magnetic probe array, which is located at (r, z)=(17.8, 80.2), consists of four pick-up probes. It measures the azimuthal characteristics of fluctuating magnetic fields with 10 *MHz* sampling rate.

3. Experimental results

Power variation experiments were employed for the systematic investigation of the rf influence on the interchange stability: (1) the power excursion, (2) power step, and (3) the power modulation. Here, results for the power excursion experiments are presented and analyzed in detail since the physical interpretation of the results of the other power variation experiments is almost identical to that of the power excursion experiments.

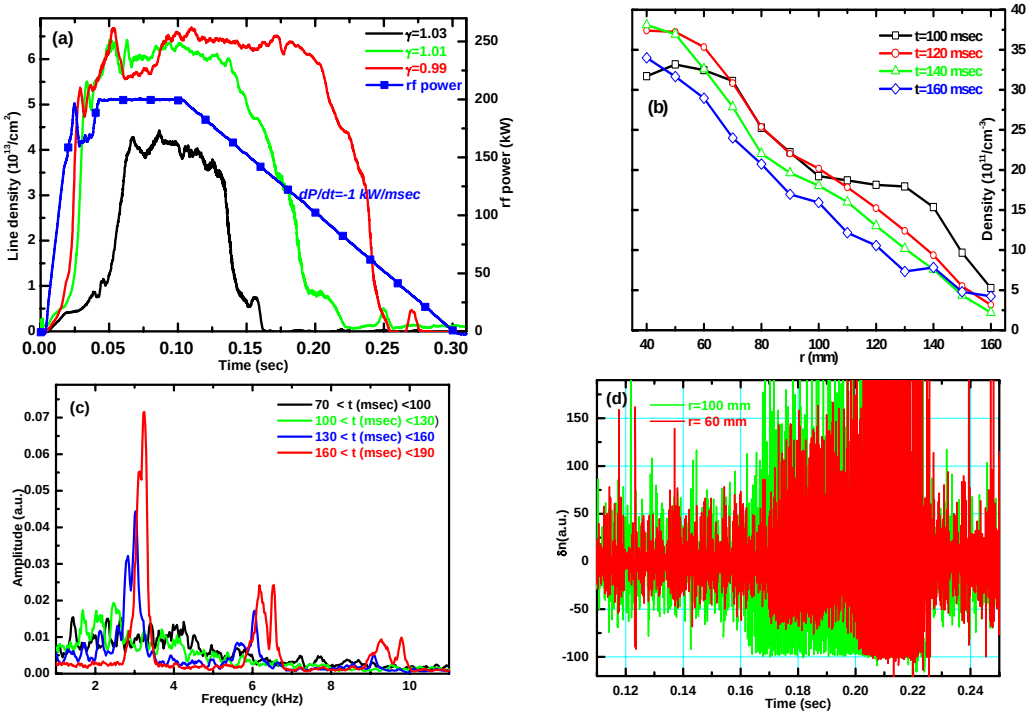

FIG. 2. (a) Time evolution of applied rf power (blue) and line averaged plasma densities for three values of $\gamma=\omega_0/\Omega_i$ *(black, green, and red lines for* γ*=1.03, 1.01, and 0.99, respectively) in power excursion experiments. Slight increase of* γ *leads to the significant reduction of the discharge*

termination time. (b) Radial density profiles at different time points during a power excursion discharge. γ=1.01 has been used. (c) Fast Fourier transform of an edge probe data in different time intervals (γ=1.01). A strong and coherent fluctuation centered at ~3 kHz starts to develop from time t≈133 msec (P_{rf} ≈167 kW). (d) Time evolution of density fluctuations at two radial positions (red:r=10.0 cm, green:r=6.0 cm).

Figure 2(a) represents time traces of the applied rf power and line averaged densities for three γ values (γ=0.99, 1.01, 1.03) during the power excursion experiments. The rf power is increased to 200 *kW* for 20 *msec*, remained flattop for 80 *msec*, and ramped down to zero with the power variation rate dP_{rf}/dt=-1 *kW/msec*. During the power excursion period, the plasma passes through the stable operation window, leading to the discharge termination when the rf power is below a threshold value as shown in Fig. 2(a). When γ is slightly larger than 1, the threshold power increases resulting in the earlier termination of the plasma discharge. Thus, the plasma is more vulnerable to the plasma termination when $\gamma \geq 1$, which confirms the empirical observations in normal discharges. Note that a slight change of γ leads to the significant change of the discharge termination time indicating the sensitivity of the operation window to the applied rf power and γ. The density profiles at various time points are given in Fig. 2(b). It shows a centrally peaked profile shape and changes little during the power excursion period.

In order to find the onset time of the plasma termination procedure and the corresponding threshold rf power, the fast Fourier transforms on edge probe data at different time intervals were carried out the results of which when γ=0.99 is shown in Fig. 2(c). A strong and coherent fluctuation centered at ~ 3 *kHz* begins to develop from *t*=133 *msec* (P_{rf}=167 *kW*). The plasma density starts to collapse ~70 *msec* after the onset of the edge fluctuation. The duration of the fluctuation prior to the beginning of the plasma termination is shortened by the decrease of γ. In power excursion experiments, this low frequency instability is usually observed to develop from the plasma edge and propagate into the core region, as indicated in Fig. 2(d) where the density fluctuation levels at two different radial positions are compared. However, in power step or modulation experiments implying the impulse variation of the rf power, it develops simultaneously across the entire plasma column.

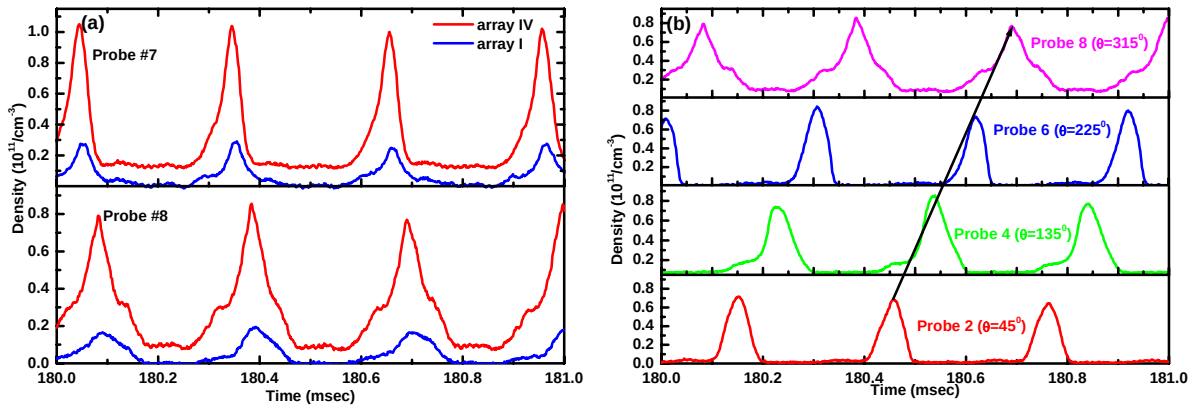

FIG. 3. Edge density fluctuations measured by (a) two probes in the same field line along the axial direction representing the flute-type mode structure, and (b) four probes in the array IV showing the mode rotation in tthe ion diamagnetic direction).

Figure 3(a) shows the density fluctuations measured by two probes at the same field line along the axial direction. The measured value of $k_{||}$ for the fluctuation is found to be zero,

indicating that it is a flute type mode. The mode rotates with ~3 *kHz* in the ion diamagnetic direction, as shown in Fig. 3(b) where the plasma densities measured by four edge probes in array IV are plotted as a function of time. Thus, the mode is identified as *m*=-1 interchange mode. This low frequency *m*=-1 interchange mode was observed for almost all the discharges ended up with a plasma termination including those given in Fig. 2(a). A similar behavior of the plasma when the interchange mode is destabilized has also been observed in GAMMA 10 tandem mirror when the anchor plasma beta is not sufficient to stabilize interchange modes in the central cell plasma[16].

A strong modulation of the high frequency rf wave with the interchange mode, and the resulting deformation of the wave envelop, which is typical phenomena in the nonlinear plasma process, was observed as shown in Fig. 4(a). Figure 4(b) represents the fast Fourier transform of the magnetic probe data, showing strong peaks at sideband frequencies $\omega_0 \pm \omega$ as well as at ω_0. The Fourier amplitude of the lower sideband has been usually observed to be stronger than that of the higher one.

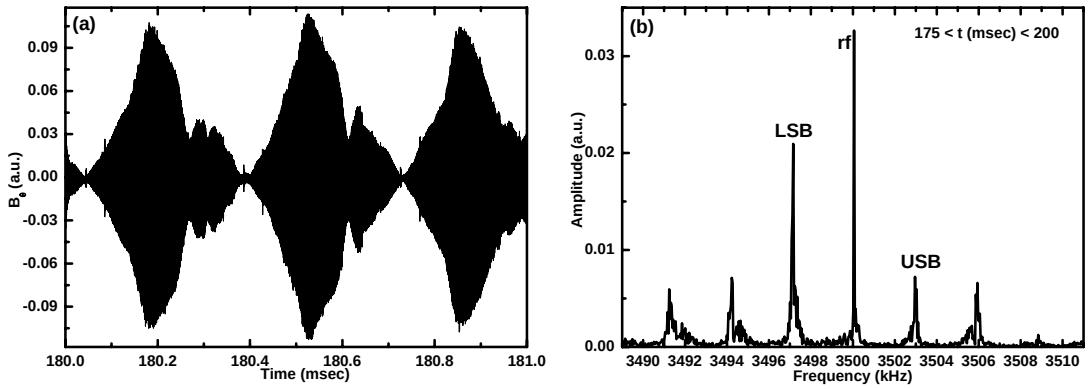

FIG. 4 (a) Fluctuating magnetic field measured by a magnetic pick-up coil showing a strong modulation of the high frequency rf wave with the interchange mode. (b) Fast Fourier transform of the magnetic probe data given in (a). Strong peaks at sideband frequencies $\omega_{\pm}=\omega_0 \pm \omega$, where ω_0 (ω) is the angular frequency of the rf wave (interchange mode), are observed.

4. Interpretation

For the interpretation of the experimental results, a local theory of the rf influence on the interchange stability in mirror plasmas has been developed taking both the EPF and the nonlinear SBC mechanism into account[17]. Effects of ion-neutral collisions were also included since they could not be neglected in HANBIT experimental conditions, as mentioned before. The theory is based on a set of two fluid equations coupled with Maxwell equations for the rf wave and electromagnetic sideband waves in the cold plasma limit. From Ref. 17, the dispersion relation for the interchange mode having wave number **k** and frequency ω is given by

$$\omega^2 + \left[(\tau - 1)\omega_{gi} + i\nu_i\right]\omega + \gamma_G^2 = \gamma_{PM}^2 \qquad (1)$$

where $\tau=T_e/T_i$, $\omega_{gi}=-kg_i/m_i\Omega_i$ with g_i representing the effective gravitational force simulating the centrifugal force originated from the field line curvature, ν_i is the ion-neutral collision frequency, $\gamma_G^2 = (k/k_n)(\tau+1)\omega_{gi}\Omega_i$, whose square root is the usual growth rate of the

interchange mode in the presence of the effective gravitational force, and $k_n \equiv \vec{\nabla} n_0 / n_0$. The γ_{PM}^2 in the right hand side of Eq. (1) represents rf effects on the interchange stability. The total rf contribution to the interchange mode is divided into the EPF part and the SBC component, $\gamma_{PM}^2 = \gamma_{SB}^2 + \gamma_{RF}^2$, where

$$\gamma_W^2 = \frac{k_n e^2}{m_i} \sum_{j=1}^{3} \sum_{\alpha} \frac{\omega_{p\alpha}^2}{\omega_{pi}^2} \frac{\left[(\omega_0 + \sigma_j \Omega_\alpha) K_{1j}^W + i \nu_\alpha K_{1j}^W\right]}{\omega_0 \left[(\omega_0 + \sigma_j \Omega_\alpha)^2 + \nu_\alpha^2\right]} |E_{\omega_0}^j|^2 \qquad (2)$$

with *W*=*SB* or *RF* denoting the contributions from sideband wave fields and pump rf wave fields, respectively. In Eq. (2), $\omega_{p\alpha}$ is the plasma frequency of the particle species α, $\sigma_{(1,2,3)}$=(-1,1,0), and $E_{\omega_0}^j$ is the rf electric field for the *j*-th component. The complication in Eq. (2) comes from the K_j^W terms the expressions of which and detailed derivations of Eqs. (1) and (2) are referred to Ref. 17.

We combined the theory with a full rf wave simulation code for a self-consistent analysis of the experimental results. The exploitation of the full wave simulation code makes it possible to incorporate the effects of the realistic antenna geometry, the conducting structures such as limiters, the axial inhomogeneity of the mirror magnetic field, the axial plasma density profile, and the inhomogeneity of rf fields in axial and radial directions. After a full rf wave simulation using experimental data, the rf fields are decomposed into Fourier components in axial direction for the stability analysis. Then, each Fourier component contributes independently to the rf-interchange mode interaction through Eq. (2).

Figure 5 shows radial intensity profiles for the *L* and *R* components of the rf electric fields. The plasma density profile and experimental conditions are taken from Fig. 1(b) at *t*=120 *msec*. Figure 5(a) represents axially averaged fields, and Fig. 5(b) indicates the dominant Fourier component in axial direction. In the present study, the rf field profiles in Fig. 5 are used for the reference stability analysis since they do not change significantly during the power excursion period.

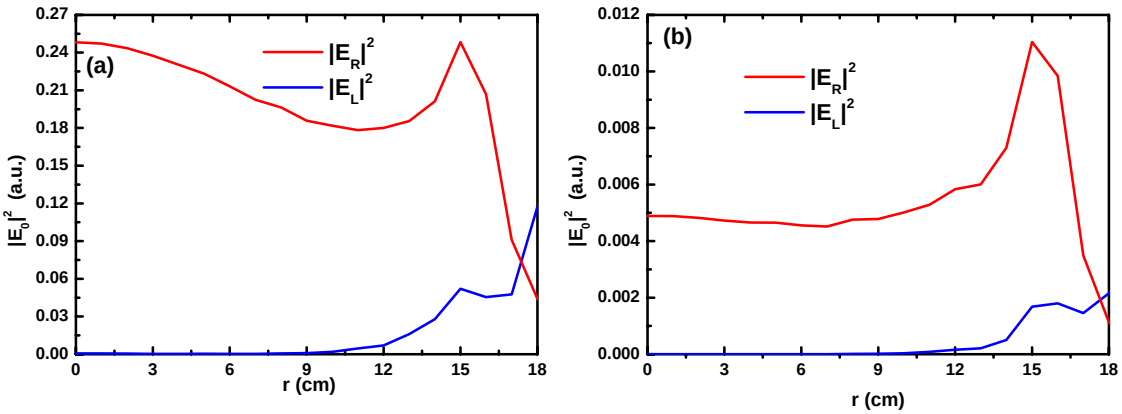

FIG. 5. L and R components of rf electric fields when γ=1.01. (a) Axially averaged and (b) one dominant Fourier component of the rf field are plotted. The plasma density profile is taken from Fig. 1(b) when t=120 msec.

Figure 6(a) shows the marginal stability boundary as functions of rf power and γ using experimental data in Fig. 1(a) and (b), and rf simulation results in Fig. 5. The rf power is normalized to 167 *kW*, which is the observed threshold power for γ=1.01. The experimental feature of the existence of the operation window in rf power and γ with the preference to γ≤1 is well reproduced in Fig. 6(a). When γ=1.01, the plasma becomes unstable as the power

decreases below a threshold value. As γ increases slightly from 1.01, the threshold power rises up substantially, making the plasma vulnerable to the interchange stability. This result is consistent with the power excursion experiment when γ=1.03. The ratio of the relative importance of EPF and SBC mechanism, $|\gamma_{SB}^2|/|\gamma_{RF}^2|$, is plotted in Fig. 6(b) as a function of *r*. As can be seen in Fig. 6(b), the nonlinear SBC process is dominant over the EPF effects for the entire plasma column except for $r\approx 0$ region where the EPM effect induced by the E_R component prevails. This leads us to the conclusion that the rf-interchange mode interaction observed in HANBIT experiments, which is performed near the resonance, is originated from the nonlinear SBC process rather than the EPF mechanism.

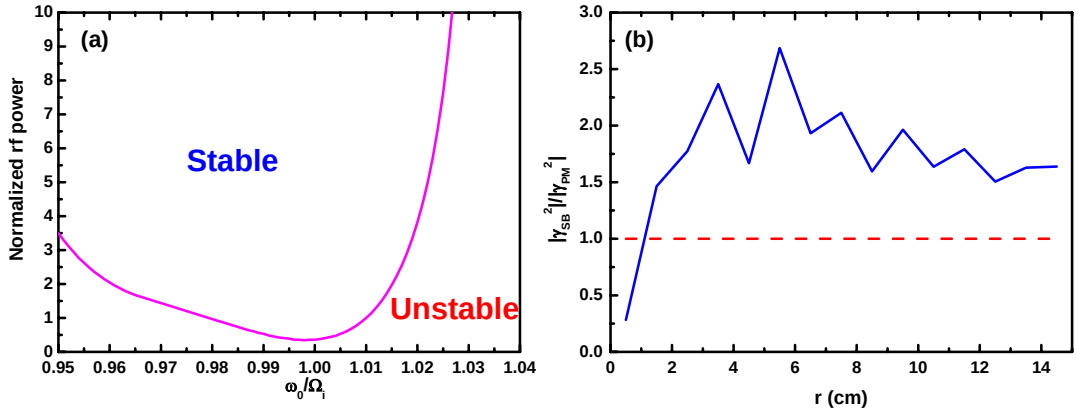

FIG. 6. (a) Marginal stability boundary for the interchange mode calculated from Eqs. (1) and (2), as functions of rf power and γ. Experimental data given in Fig. 1(a) and (b) when γ=1.01 and rf simulation results in Fig. 5 have been used. The existence of interchange-stable operation window as a function of rf power and γ with the preference to γ≤1 is reproduced. (b) $|\gamma_{SB}^2|/|\gamma_{RF}^2|$ *as a function of r. The SBC process is the dominant rf-interchange mode interaction mechanism for the entire plasma column.*

5. Conclusions

We observed the interchange-stable operation window in a rf-heated mirror plasma due to the strong nonlinear interaction between the interchange mode and the pump rf wave. The operation window is a sensitive function of the applied rf power and $\gamma=\omega_0/\Omega_i$ with the preference of $\gamma \leq 1$. The energy transfer mechanism between the four waves involved in the nonlinear interaction and the physical origin of the observed bulk rotation when the interchange mode becomes unstable will be subjects for future investigation.

* This work was supported by the Ministry of Korean Science and Technology under the HANBIT project contract.

[1] J. R. Ferron, N. Hershkowitz, R. A. Breun, S. N. Golovato, and R. Goulding, Phys Rev. Lett. **51** (1983) 1955.
[2] Y. Yasaka and R. Itatani, Phys. Rev. Lett. **56** (1986) 2811.
[3] R. Majeski, J. J. Browning, S. Meassick, N. Hershkowitz, T. Intrator, and J. R. Ferron, Phys. Rev. Lett. **59** (1987) 206.
[4] J. J. Browning, R. Majeski, T. Intrator, N.Hershkowitz, and S. Meassick, Phys. Fluids **31** (1988) 714.
[5] J. J. Browning, N. Hershkowitz, T. Intrator, R. Majeski, and S. Meassick, Phys. Fluids B **1**, (1989) 1692.

[6] J. R. Myra and D. A. D'Ippolito Phys. Rev. Lett. **53** (1984) 914.
[7] D. A. D'Ippolito and J. R. Myra, Phys. Fluids **28** (1985) 1895.
[8] J. B. McBride, Phys. Fluids **27** (1984) 324.
[9] J. B. McBride, V. Stefan, and N. A. Krall, Phys. Rev. Lett. **54** (1985) 42.
[10] P. L. Similon and A. N. Kaufman Phys. Rev. Lett. **53** (1984) 1061.
[11] D. A. D'Ippolito and J. R. Myra, Phys. Fluids **29** (1986) 2594.
[12] S. Meassick, T. Intrator, N. Hershkowitz, J. J. Browning, and R. Majeski, Phys. Fluids B **1** (1989)1049.
[13] M. Kwon *et. al*., Fusion Sci. Technol. **43(1T)** (2003) 23.
[14] B. H. Park, N. S. Yoon, S. S. Kim, J. Y. Kim, and M. Kwon, Fusion Sci. Technol. **43(1T)** (2003) 92.
[15] S. G. Lee, J. G. Bak, S. J. Jeon, S. S. Kim, and H. K. Na, Fusion Sci. Technol. **43(1T)** (2003) 248.
[16] R. Minami, T. Cho, J. Kohagura, M. Hirata *et al.*, Plasma Phys. Control. Fusion, **44** (2002) 1363.
[17] S. S. Kim and H. Jhang, Phys. Plasmas, **11** (2004) 4088.